

Iterative deblending of simultaneous-source seismic data using seislet-domain shaping regularization

Yangkang Chen¹, Sergey Fomel¹, and Jingwei Hu¹

ABSTRACT

We used a novel iterative estimation scheme for separation of blended seismic data from simultaneous sources. The scheme is based on an augmented estimation problem that can be solved by iteratively constraining the deblended data using shaping regularization in the seislet domain. We formulated the forward modeling operator in the common-receiver domain, in which two sources were assumed to be blended using a random time-shift dithering approach. The nonlinear shaping-regularization framework offered some freedom in designing a shaping operator to constrain the model in an underdetermined inverse problem. We designed the backward operator and the shaping operator for the shaping-regularization framework. The backward operator can be optimally chosen as half of the identity operator in the two-source case, and the shaping operator can be chosen as coherency-promoting operator. The high performance deblending effect of the iterative framework was tested on three numerically blended synthetic data sets and one numerically blended field data set. Compared with alternative f - k domain thresholding and f - x predictive filtering, seislet-domain soft thresholding exhibits the most robust behavior.

INTRODUCTION

The simultaneous-source technique aims at removing the limitation of no interference between adjacent shots by allowing more than one source to be shot simultaneously. Thus, it can reduce the acquisition period and increase spatial sampling (Berkhout, 2008). Because of its economic benefits and technical challenges, this technique has attracted significant attention of researchers in industry and academia (Moore et al., 2008; Mahdad et al., 2011; Abma et al.,

2012; Huo et al., 2012; Wapenaar et al., 2012). The biggest issue involved in simultaneous-source processing is intense crosstalk noise between adjacent shots, which poses a challenge for conventional processing. One way to deal with this issue is to use a first-separate and second-process strategy, which is also known as deblending (Doulgeris et al., 2012). The other way is by direct imaging and waveform inversion (Berkhout et al., 2012; Choi and Al Khalifah, 2012; Guitton and Diaz, 2012; Plessix et al., 2012; Xue et al., 2014). In this paper, we focus on the deblending approach.

Different filtering and inversion methods have been applied previously to deblend seismic data. Filtering methods use the property that the coherency of the simultaneous-source data varies in different domains. Therefore, one can get unblended data by filtering out randomly distributed blending noise in some transform domains, where one source record is coherent and the others are not (Hampson et al., 2008; Huo et al., 2012; Mahdad et al., 2012). Inversion methods treat the separation problem as an estimation problem that aims at estimating the desired unknown unblended data. Because of the ill-posed nature of such estimation problems, a regularization term is usually required (Doulgeris et al., 2012). The regularization term can be chosen as a sparsity promotion in a sparsifying transformed domain (Abma et al., 2010). Van Borselen et al. (2012) proposed to distribute all energy in the shot records by reconstructing individual shot records at their respective locations. Mahdad et al. (2011) introduced an iterative estimation and subtraction scheme that combines the properties of filtering and inversion methods and exploits the fact that the characteristics of the blending noise differ in different domains. One choice is to transform seismic data from the common-shot domain to common-receiver, common-offset, or CMP domain. Beasley et al. (2012) proposed a separation technique called the alternating projection method, and demonstrated it to be robust in the presence of aliasing.

In this paper, we propose a novel iterative estimation scheme for the separation of blended seismic data. We construct an augmented estimation problem, then use shaping regularization (Fomel, 2007,

Manuscript received by the Editor 2 December 2013; revised manuscript received 13 May 2014; published online 5 August 2014.

¹The University of Texas at Austin, Bureau of Economic Geology, John A. and Katherine G. Jackson School of Geosciences, Austin, Texas, USA. E-mail: ykchen@utexas.edu; sergey.fomel@beg.utexas.edu; hu@ices.utexas.edu.

© 2014 Society of Exploration Geophysicists. All rights reserved.

2008) to constrain the characteristics of the model during the iteration process for obtaining a suitable estimation result. We adopt seislet-domain (Fomel and Liu, 2010) soft thresholding as a robust shaping operator to remove crosstalk noise and at the same time to preserve useful components of seismic data. Shaping regularization maps each model into a more admissible model at each iteration and allows us to solve the deblending problem with a small number of iterations.

This paper is organized as follows: We first present a formulation of numerical blending using an augmented block-matrix equation. We then incorporate shaping regularization to solve the forward equation iteratively and discuss the selection of the backward operator and shaping operator involved in the shaping-regularization iterative framework. Finally, we test the proposed iterative framework on three numerically blended synthetic data sets and one numerically blended field data set and compare three different choices of the shaping operator: f - k domain thresholding, f - x predictive filtering, and seislet-domain thresholding.

DEBLENDING USING SHAPING REGULARIZATION

Numerical blending

We assume that the seismic record is blended using two independent sources that correspond to two shooting vessels in the ocean-bottom node (OBN) acquisition (Mitchell et al., 2010). Here, one source means a collection of shots from one shooting vessel. The two sources shoot pseudosynchronously, which means that each shot in one source has a random time dithering compared with the corresponding shot in another source. By precisely picking the shooting time of each shot of one source at the long seismic record on the node, we can get one common-receiver gather. Using the second source, we get another gather. Thus, the forward problem can be formulated as follows:

$$\mathbf{d} = \mathbf{d}_1 + \mathbf{T}\mathbf{d}_2. \quad (1)$$

Here, \mathbf{d}_1 and \mathbf{d}_2 denote the seismic records to be separated out, \mathbf{d} is the blended data, and \mathbf{T} denotes the dithering operator. Note that, we perform the processing in the common-receiver domain because each blended record in this domain is coherent for one source and incoherent for another (Hampson et al., 2008). In this case, \mathbf{d} is usually referred to as the pseudodeblended data (Mahdad et al., 2011), which means picking traces from the original blended field record according to the shooting time of one source to form a common-receiver gather with one source coherent and the other one incoherent. We propose to augment equation 1 with another equation through applying the inverse dithering operator \mathbf{T}^{-1} :

$$\mathbf{T}^{-1}\mathbf{d} = \mathbf{T}^{-1}\mathbf{d}_1 + \mathbf{d}_2. \quad (2)$$

By combining equations 1 and 2, we formulate an augmented estimation problem:

$$\mathbf{Fm} = \tilde{\mathbf{d}}, \quad (3)$$

where

$$\tilde{\mathbf{d}} = \begin{bmatrix} \mathbf{d} \\ \mathbf{T}^{-1}\mathbf{d} \end{bmatrix}, \quad \mathbf{F} = \begin{bmatrix} \mathbf{I} & \mathbf{T} \\ \mathbf{T}^{-1} & \mathbf{I} \end{bmatrix}, \quad \mathbf{m} = \begin{bmatrix} \mathbf{d}_1 \\ \mathbf{d}_2 \end{bmatrix}, \quad (4)$$

and \mathbf{I} is the identity operator.

We choose to solve equation 3 rather than equation 1 because equation 3 is a more convenient form to use in the following derivations.

Shaping regularization

The unknown \mathbf{m} in equation 3 can be recovered iteratively using shaping regularization:

$$\mathbf{m}_{n+1} = \mathbf{S}[\mathbf{m}_n + \mathbf{B}(\tilde{\mathbf{d}} - \mathbf{F}\mathbf{m}_n)], \quad (5)$$

where operator \mathbf{S} shapes the estimated model into the space of admissible models at each iteration (Fomel, 2007, 2008) and \mathbf{B} is the backward operator that provides an inverse mapping from data space to model space. Daubechies et al. (2004) prove that, if \mathbf{S} is a nonlinear thresholding operator (Donoho and Johnstone, 1994), $\mathbf{B} = \mathbf{F}^T$, where \mathbf{F}^T is the adjoint operator of \mathbf{F} , iteration 5 converges to the solution of equation 6 with L_1 regularization term:

$$\min_{\mathbf{m}} \|\mathbf{Fm} - \tilde{\mathbf{d}}\|_2^2 + \mu \|\mathbf{A}^{-1}\mathbf{m}\|_1, \quad (6)$$

where μ is the threshold and \mathbf{A}^{-1} denotes a sparsity-promoting transform. A better choice for \mathbf{B} is the pseudoinverse of \mathbf{F} : $\mathbf{B} = (\mathbf{F}^T\mathbf{F})^{-1}\mathbf{F}^T$ (Daubechies et al., 2008).

Performance evaluation and convergence rate

Combining equations 3–5, we get

$$\begin{bmatrix} \mathbf{d}_1 \\ \mathbf{d}_2 \end{bmatrix}_{n+1} = \mathbf{S} \left[\begin{bmatrix} \mathbf{d}_1 \\ \mathbf{d}_2 \end{bmatrix}_n + \mathbf{B} \left[\begin{bmatrix} \mathbf{d} \\ \mathbf{T}^{-1}\mathbf{d} \end{bmatrix} - \begin{bmatrix} \mathbf{I} & \mathbf{T} \\ \mathbf{T}^{-1} & \mathbf{I} \end{bmatrix} \begin{bmatrix} \mathbf{d}_1 \\ \mathbf{d}_2 \end{bmatrix}_n \right] \right], \quad (7)$$

where \mathbf{S} is a block operator that takes the form $[\mathbf{S}_1 \quad \mathbf{0}; \mathbf{0} \quad \mathbf{S}_2]$, and \mathbf{S}_1 and \mathbf{S}_2 correspond to the shaping operators for \mathbf{d}_1 and \mathbf{d}_2 , respectively. Using equation 7 and performing appropriate iterations, we aim to get an estimate of unblended seismic data.

To test the convergence performance and accuracy of iteration 7, we use the following measure (Hennenfent and Herrmann, 2006):

$$S/N_{i,n} = 10 \log_{10} \frac{\|\mathbf{d}_i\|_2^2}{\|\mathbf{d}_i - \mathbf{d}_{i,n}\|_2^2}, \quad (8)$$

where $S/N_{i,n}$ stands for signal-to-noise ratio of i th source after n th iteration, $\mathbf{d}_{i,n}$ denotes the estimated model of i th source after n iterations, \mathbf{d}_i denotes the true model for i th source and $\|\cdot\|_2^2$ denotes the squared L_2 norm of a function.

BACKWARD OPERATOR

In equation 5, \mathbf{B} is an approximate inverse of \mathbf{F} . Recall that the dithering operator applies a time-domain random time shift to the input seismic data. Taken in the frequency domain, the dithering operator takes the following form:

$$\mathbf{T} = \mathcal{F}^{-1} \mathbf{P} \mathcal{F}, \quad (9)$$

where \mathcal{F} and \mathcal{F}^{-1} are forward and inverse Fourier transforms, respectively, and \mathbf{P} is an $N \times N$ diagonal block phase-shift operator given by

$$\mathbf{P} = \text{diag}(\mathbf{P}_1, \mathbf{P}_2, \mathbf{P}_3, \dots, \mathbf{P}_N), \quad (10)$$

where \mathbf{P}_n denotes the individual phase shift operator for n th trace and can be expressed as an $M \times M$ diagonal matrix:

$$\mathbf{P}_n = \text{diag}(\overbrace{1, 1, 1, \dots, 1}^M) * \exp(-i\omega\delta t_n). \quad (11)$$

Here, ω denotes the angular frequency, δt_n denotes the random dithering time of n th trace, M and N in equations 10 and 11 denote the number of temporal samples and number of traces, respectively, and $\text{diag}(\cdot)$ denotes a diagonal matrix.

Considering that the Fourier operator (with symmetric normalization) and the phase shift operator are both unitary, which means $\mathcal{F}^{-1} = \mathcal{F}^T$ and $\mathbf{P}^{-1} = \mathbf{P}^T$, it is easy to see that

$$\mathbf{T}^T = (\mathcal{F}^{-1} \mathbf{P} \mathcal{F})^T = \mathcal{F}^T \mathbf{P}^T \mathcal{F} = (\mathcal{F}^{-1} \mathbf{P} \mathcal{F})^{-1} = \mathbf{T}^{-1}. \quad (12)$$

Thus, we conclude that the dithering operator is also a unitary operator. Furthermore we notice that

$$\mathbf{F}^T = \begin{bmatrix} \mathbf{I} & \mathbf{T} \\ \mathbf{T}^{-1} & \mathbf{I} \end{bmatrix}^T = \begin{bmatrix} \mathbf{I} & \mathbf{T}^{-T} \\ \mathbf{T}^T & \mathbf{I} \end{bmatrix} = \begin{bmatrix} \mathbf{I} & \mathbf{T} \\ \mathbf{T}^{-1} & \mathbf{I} \end{bmatrix} = \mathbf{F}$$

and

$$\mathbf{F}^T \mathbf{F} = \begin{bmatrix} \mathbf{I} & \mathbf{T} \\ \mathbf{T}^{-1} & \mathbf{I} \end{bmatrix} \begin{bmatrix} \mathbf{I} & \mathbf{T} \\ \mathbf{T}^{-1} & \mathbf{I} \end{bmatrix} = 2 \begin{bmatrix} \mathbf{I} & \mathbf{T} \\ \mathbf{T}^{-1} & \mathbf{I} \end{bmatrix} = 2\mathbf{F}. \quad (13)$$

The least-squares solution of equation 3 is therefore

$$\hat{\mathbf{m}} = (\mathbf{F}^T \mathbf{F})^{-1} \mathbf{F}^T \tilde{\mathbf{d}} = \frac{1}{2} \mathbf{F}^{-1} \mathbf{F}^T \tilde{\mathbf{d}} = \frac{1}{2} \tilde{\mathbf{d}}. \quad (14)$$

According to equation 14, an appropriate choice for \mathbf{B} is $\mathbf{B} = \frac{1}{2} [\mathbf{I} \ 0; 0 \ \mathbf{I}]$. This form of the derived backward operator is also referred to as *scaled pseudodeblending* (Mahdad, 2012).

The dithering operator is unitary only if the time-shift range is small, and so the constructive summation of the useful components (events) between different traces can be ignored. Even if this condition is not fully met, we can use the concept of interference to generalize the meaning of the dithering operator \mathbf{T} . Although, in this case, the backward operator might not be most appropriately chosen as half of the identity operator, we can still use it as an approximation.

SHAPING OPERATOR

The shaping operator \mathbf{S} in equation 5 can be chosen as a coherency-promoting operator, which serves as a flexible constraint on the estimated model. Any coherency-promoting tool such as f - x predictive filtering (Canales, 1984; Sacchi and Kuehl, 2000;

Galbraith and Yao, 2012; Chen and Ma, 2014) or median filter (Liu et al., 2009b; Huo et al., 2012; Liu, 2013) can be used to preserve the coherent useful subsurface reflection and at the same time to remove incoherent blending noise.

Another approach to promote coherency is to promote sparseness in an appropriate transform domain. To enforce sparsity, a transform domain thresholding operation can also be chosen as the shaping operator as long as the data in the transformed domain are sparse (Mallat, 2009; Candes and Plan, 2011). Instead of a thresholding operator, we can also use a mask operator to compress the transformed domain (Naghizadeh and Sacchi, 2010; Liu and Fomel, 2012). A sparsity-promoting shaping operator can be defined as

$$\mathbf{S}_i = \mathbf{A} \mathcal{T}_{\gamma_i} [\mathbf{A}^{-1}], \quad (15)$$

where i denotes the i th source, \mathbf{A}^{-1} and \mathbf{A} are forward and inverse sparsity-promoting transforms, and \mathcal{T}_{γ_i} corresponds to a mask operator or thresholding operator with an input parameter γ_i in the transformed domain.

Mask operator can be chosen to preserve small-scale components and remove large-scale components. It takes the following form:

$$\mathcal{M}_{\gamma_i}(v(\mathbf{x})) = \begin{cases} v(\mathbf{x}) & \text{for } s(\mathbf{x}) < \gamma_i, \\ 0 & \text{for } s(\mathbf{x}) \geq \gamma_i \end{cases}, \quad (16)$$

where \mathbf{x} is a position vector in the transformed domain, $v(\mathbf{x})$ denotes the amplitude value of point \mathbf{x} , $s(\mathbf{x})$ denotes the scale of point \mathbf{x} , and \mathcal{M}_{γ_i} corresponds to the mask operator with a scale limitation γ_i . When the sparsity-promoting transform is the Fourier transform, the scale defined in the mask operator shown in equation 16 corresponds to the frequency and wavenumber band.

Thresholding operators can be divided into two types: soft and hard thresholding. Soft thresholding or shrinkage aims to remove data whose value is smaller than a certain level and subtract the other data values by this level (Donoho, 1995). Hard thresholding removes data with small values. A soft thresholding operator takes the following form:

$$\mathcal{S}_{\gamma_i}(v(\mathbf{x})) = \begin{cases} v(\mathbf{x}) - \gamma_i \frac{v(\mathbf{x})}{|v(\mathbf{x})|} & \text{for } |v(\mathbf{x})| > \gamma_i, \\ 0 & \text{for } |v(\mathbf{x})| \leq \gamma_i \end{cases}, \quad (17)$$

where \mathcal{S}_{γ_i} corresponds to the soft thresholding operator with a threshold value γ_i .

Similarly, a hard thresholding operator takes the form

$$\mathcal{H}_{\gamma_i}(v(\mathbf{x})) = \begin{cases} v(\mathbf{x}) & \text{for } |v(\mathbf{x})| > \gamma_i, \\ 0 & \text{for } |v(\mathbf{x})| \leq \gamma_i \end{cases}, \quad (18)$$

where \mathcal{H}_{γ_i} corresponds to the hard thresholding operator with a threshold value γ_i .

The mask operator can be more efficient because it is linear and requires only the scale coefficient below which data values are preserved. The thresholding operator needs to compare the amplitude value of each transformed domain point with a predefined coefficient. However, the mask operator is more difficult to design when the signal and noise coefficients are both spread across the transformed domain. Therefore, in the case of deblending, we prefer to use the thresholding operator rather than the mask operator. The selection criteria of γ_i in the above definitions of thresholding

operators (soft and hard) leads to different kinds of thresholding strategies, which may result in different thresholding performances (convergence rate and quality) (Yang et al., 2013). Some of the common iterative thresholding strategies are constant-value thresholding, linear-decreasing thresholding, exponential-decreasing thresholding, etc. (Gao et al., 2010). In our paper, we use percentile thresholding (Wang et al., 2008; Yang et al., 2012), which is convenient to implement and helps to accelerates the convergence (Yang et al., 2012).

Comparison of sparsity-promoting transforms

The best-known sparsity-promoting transforms are the Fourier and wavelet transforms. Fomel and Liu (2010) propose a sparsity-promoting transform called seislet transform. The specific

adaptation for seismic data makes the seislet transform appealing to seismic data processing. In the seislet domain, useful events and blending noise reside at different scales and the useful signal tends to form a more compact region. We provide a brief review of the seislet transform in Appendix A.

To illustrate the comparative sparseness of different transforms, we first create a simple synthetic data (Figure 1). Figure 2 shows different transformed domains for the data. Figure 2d shows a comparison between the decay of sorted coefficients in the 2D Fourier transform, 2D wavelet transform, and 2D seislet transform. The 2D Fourier transform in this case means the $f\text{-}k$ transform. The 2D wavelet transform means implementing the 1D wavelet transform along the temporal direction first and along the spatial direction second. The 2D seislet transform means implementing the seislet transform along the spatial direction first and 1D seislet transform along the temporal direction second. Our experiments show that the seislet coefficients decay significantly faster than coefficients of the other two transforms, which indicates a more compact structure of the seislet domain. The shaping operation is thus preferably chosen as the thresholding or mask operation in the seislet domain.

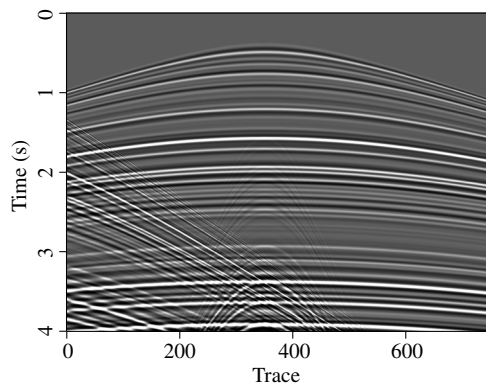


Figure 1. A synthetic seismic profile.

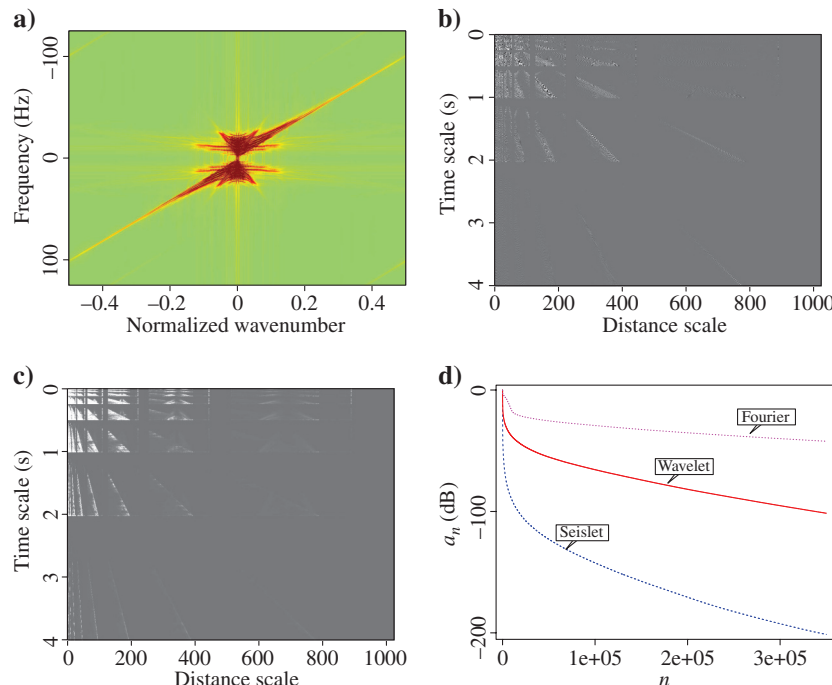


Figure 2. Comparison among different sparsity-promoting transforms. (a) 2D Fourier transform domain, (b) 2D wavelet transform domain, (c) 2D seislet transform domain, and (d) coefficients decreasing diagram.

EXAMPLES

In this section, to test the effectiveness of the proposed iterative framework defined in equation 5, we create three numerically blended examples with different kinds of shaping operations. The iterative framework in equation 5 is fundamentally a noise attenuation algorithm. The better an operator's ability to remove blending noise and preserve useful signal, the more appropriate it is for shaping. From this point of view, we first created two synthetic sections in different cases. One is a linear event case, with conflicting dip components, and the other is a hyperbolic event case, without crossing events. To deal with a more realistic and difficult situation, we created a more complex synthetic model (shown in Figure 1 and used previously for comparing the sparseness of different transforms) to test the proposed deblending algorithm. For the field data example, we use two common-receiver gathers acquired by the OBN technique to generate a numerically blended data test.

The first three blended synthetic data sets (shown in Figures 3–11) show almost perfect deblending results, particularly when the shaping operator is chosen as soft thresholding in the seislet domain. The third blended synthetic data set shows an acceptable result only for seislet-domain soft thresholding. The blended field data example also shows an acceptable deblending result using seislet-domain soft thresholding. All experiments are based on an OBN acquisition, as noted in the beginning of the paper. Thus, each seismic section in the examples corresponds to a common-receiver gather. The first example is used for testing the denoising ability of each of the shaping operators in the case of crossing events. This example can also demonstrate the deblending performance for common-offset gathers, where most seismic events are linear.

For conciseness, we show the deblending performance for only one source.

Numerically blended synthetic data — Linear events

Our first synthetic example contains three plane-wave events, with one high-dip angle event crossing two other events. The original unblended and numerically blended sections are shown in Figure 3a and 3b, respectively. Figure 4 shows the deblended results using soft thresholding in the $f\text{-}k$ domain, soft thresholding in the seislet domain, and $f\text{-}x$ predictive filtering. All

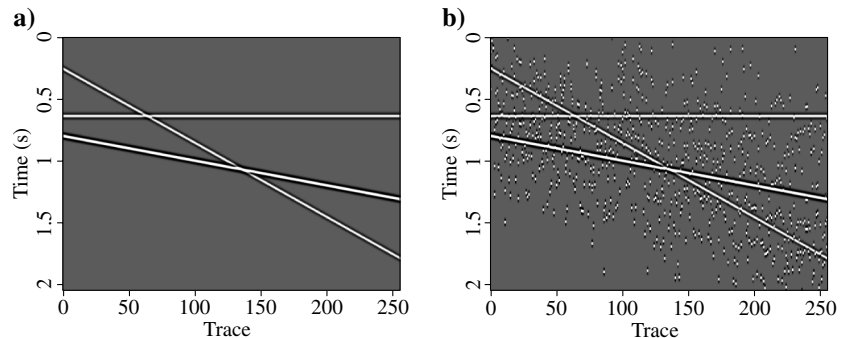


Figure 3. Numerically blended synthetic data (linear case). (a) Unblended data and (b) blended data.

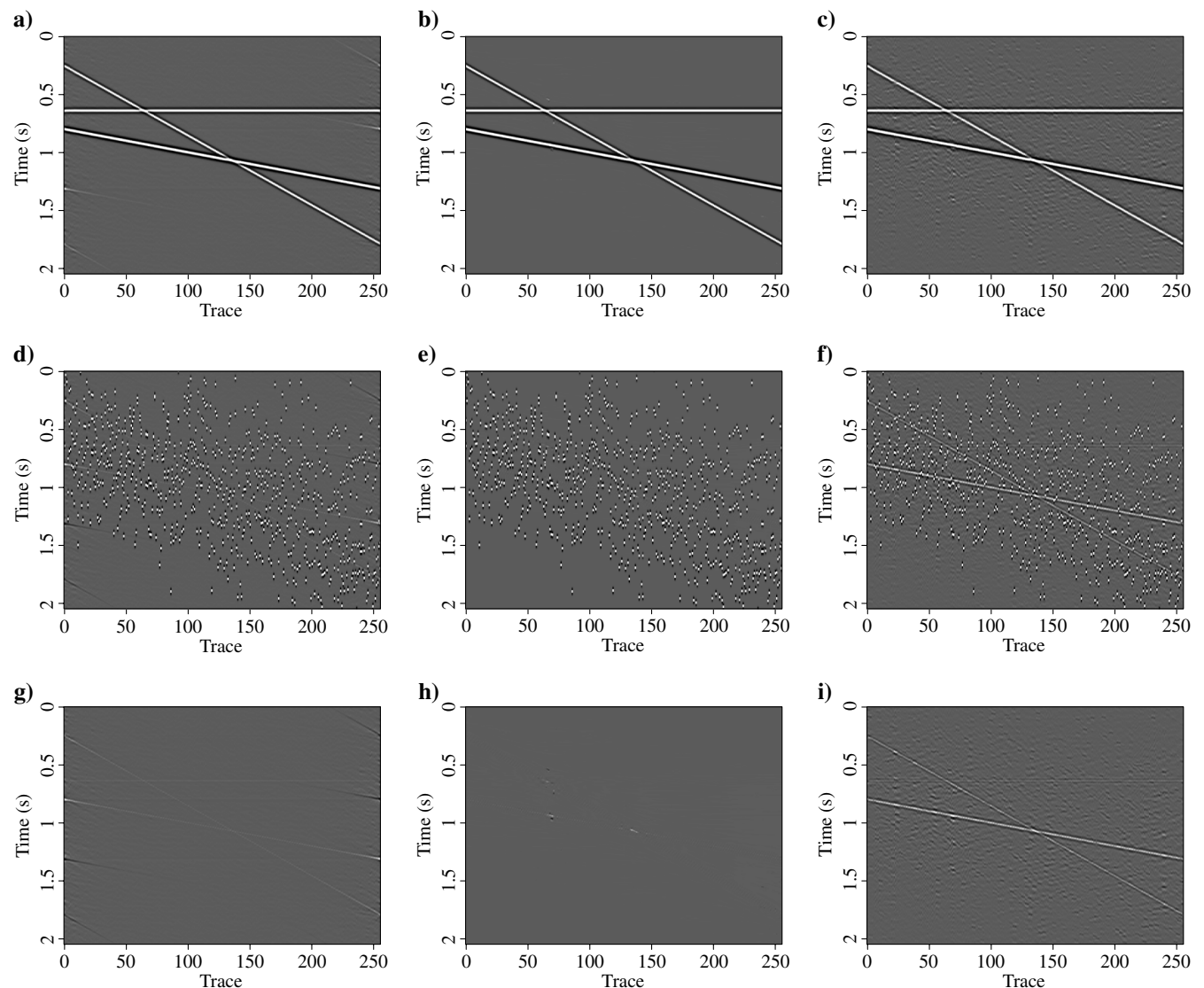


Figure 4. Deblending comparison for numerically blended synthetic data (linear case). (a) Deblended result using $f\text{-}k$ domain thresholding, (b) deblended result using seislet-domain thresholding, (c) deblended result using $f\text{-}x$ predictive filtering, (d) blending noise corresponding to (a), (e) blending noise corresponding to (b), (f) blending noise corresponding to (c), (g) estimation error corresponding to (a), (h) estimation error corresponding to (b), and (i) estimation error corresponding to (c).

of these deblending results are generally acceptable despite some artifacts left in Figure 4a and some weak-level noise left in Figure 4c. By computing the difference between the deblended and the blended section, we can obtain the blending noise section. Comparing the blending noise sections (see Figure 4d–4f), we find that there is some leakage of useful energy for f - x predictive filtering. Computing the differences between the deblended and the unblended sections, we get the estimation error sections, shown in Figure 4g–4i. Compared with the other two shaping approaches, seislet-domain soft thresholding causes an almost zero estimation error, which indicates an almost perfect deblending result. The estimation error for f - x predictive filtering is comparatively large because of the large predictive error problem when several dipping components are taken into consideration (Chen and Ma, 2014). The small estimation errors in Figure 4g are caused by spectrum mixture in the f - k domain because some useful energy reside in the low-amplitude part that is easy to be removed during soft thresholding. The small estimation errors shown in Figure 4h are caused by dip estimation error because of the conflicting dips when using the plane-wave destruction (PWD) algorithm with a single slope (Fomel, 2002), which is a limitation of seislet-domain denoising approaches, unless a seislet frame is used instead of the seislet transform (Fomel and Liu, 2010). The diagrams for convergence rates are shown in Figure 5, which demonstrates a superior behavior of

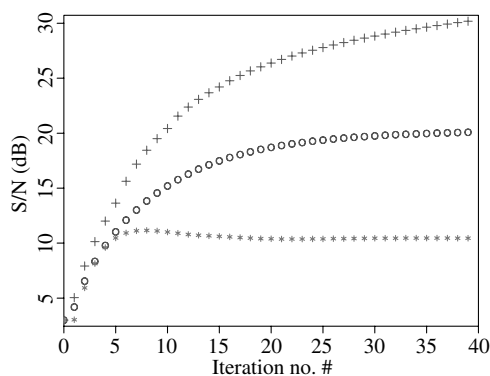


Figure 5. Diagrams of S/N for synthetic example (linear case). The + line corresponds to seislet-domain thresholding, the o line corresponds to f - k domain soft thresholding, and the * line corresponds to f - x predictive filtering.

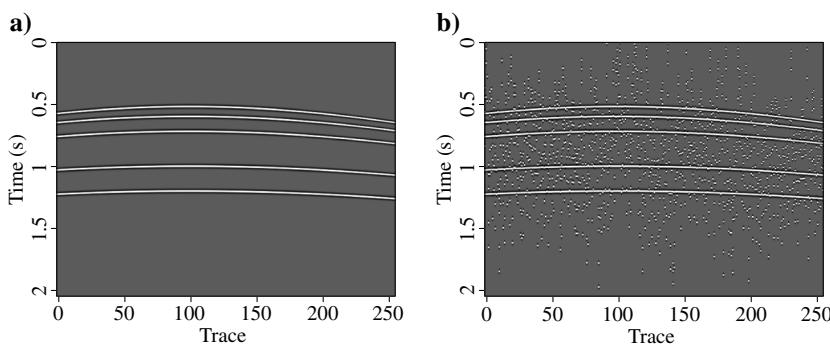


Figure 6. Numerically blended synthetic data (hyperbolic case). (a) Unblended data and (b) blended data.

seislet-domain soft thresholding in comparison with the other two approaches. To make the comparisons fair, we try to find the best deblending performance through the parameter-selection process for corresponding shaping operators. In this case, the percentages we use for f - k domain and seislet-domain thresholding are both 8%, the filter length we use for f - x predictive filtering is four samples.

Numerically blended synthetic data — Hyperbolic events

Next, we create another synthetic example which contains hyperbolic events without dip conflicts. The unblended and blended data are shown in Figure 6a and 6b, respectively. Figure 7 shows the deblending results for the hyperbolic case. Figure 8 shows the diagrams of the changing S/N for one source. In this case, the estimation error for the seislet-domain soft thresholding becomes negligible, mainly owing to the successful dip estimation when constructing the seislet transform. The strength of the f - x predictive filtering also increases and its S/N diagram shows a similar behavior as the f - k domain thresholding. The seislet-based shaping still outperforms the other two approaches. In this case, the percentages we use for f - k domain and seislet-domain thresholding are both 9%, the filter length we use for f - x predictive filtering is four samples.

Numerically blended synthetic data — Complex gather

The third synthetic data set consists of two complex gathers, which contain useful seismic reflections and additional components such as ground roll and coherent dipping events. We simulate this example to best match the field data. The unblended and blended data are shown in Figure 9, respectively. Figure 10 shows the diagrams of changing S/N for both sources. The S/N for the converged deblended data becomes noticeably smaller compared with the previous examples for three different shaping operators, respectively, which results from the fact that the seismic gather is no longer ideally sparse as the previous examples. Notice that in the noise sections for f - k domain thresholding (Figure 10a) and the noise sections for f - x predictive filtering (Figure 10c), there exist a certain amount of coherent events. However, for the seislet-domain soft thresholding, there are barely any coherent events. If we look carefully at the error sections corresponding to these three shaping operators, we can find that for the f - k domain thresholding, the estimation error comes from the useful hyperbolic reflections, the coherent dipping events, and the ground roll for the f - x predictive filtering.

The estimation error mainly comes from the useful hyperbolic reflections and the coherent dipping events, but for the seislet-domain soft thresholding, only a small amount of the ground roll and negligible amount of coherent dipping events and deep water horizontal reflections are left on the error sections, which is not important for the whole processing tasks. We can conclude that for complex data sets like this synthetic example, seislet-domain soft thresholding is the preferable approach for shaping regularization. In this case, the percentages we use for the f - k domain and seislet-domain thresholding are both 20%, the filter length we use for f - x predictive filtering is four samples.

Numerically blended field data

Finally, we use a field data example to further test the effectiveness for our proposed algorithm. The field data are similar in appearance to the previous synthetic example. Because of the previous test, we only used seislet-domain soft thresholding as the shaping operator. The two blended data are shown in Figure 12a and 12b and appear noisy. After 30 iterations of seislet-domain soft thresholding, the deblending results are shown in Figure 12d and 12c. The intense interference in the shallow part has been removed to a large extent. The deep water reflection becomes much clearer because of a significant drop in the noise energy for the whole profile. From the noise sections, we can observe only a small amount of ground roll, which is analogous to the results of the previous synthetic test, and an even smaller amount of direct waves and shallow part horizontal reflections, which is not significant. The S/N defined in equation 8

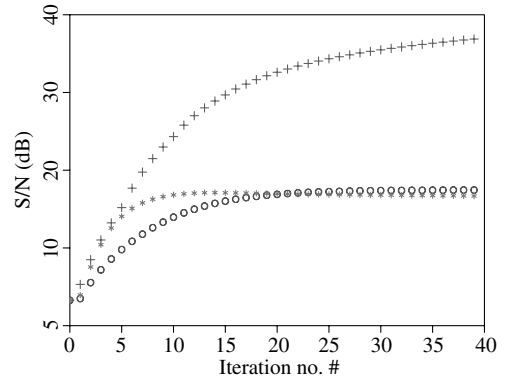


Figure 8. Diagrams of S/N for synthetic example (hyperbolic case). The + line corresponds to seislet-domain thresholding, the o line corresponds to $f\text{-}k$ domain thresholding, and the * line corresponds to $f\text{-}x$ predictive filtering.

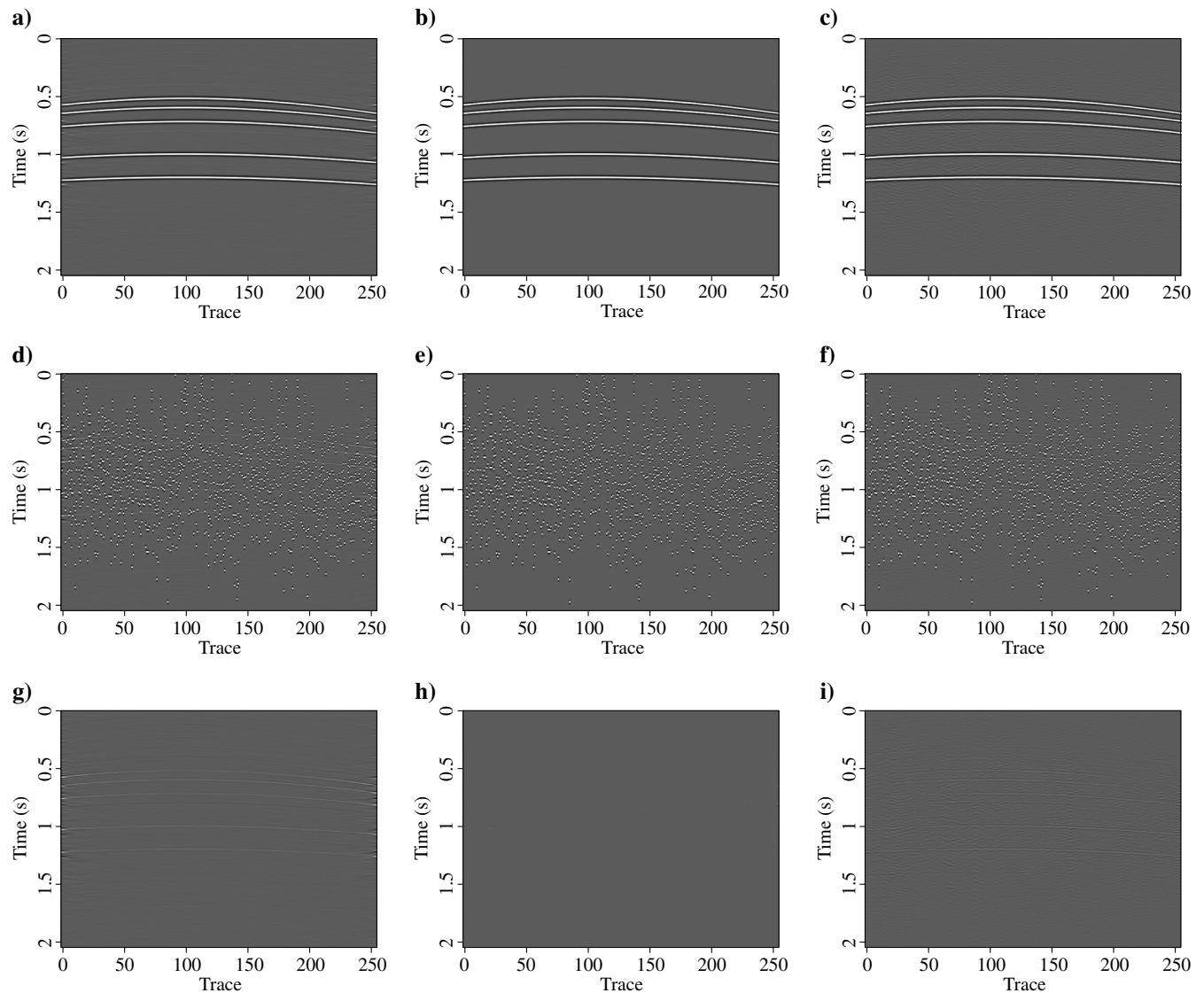


Figure 7. Deblending comparison for numerically blended synthetic data (hyperbolic case). (a) Deblended result using $f\text{-}k$ domain thresholding, (b) deblended result using seislet-domain thresholding, (c) deblended result using $f\text{-}x$ predictive filtering, (d) blending noise corresponding to (a), (e) blending noise corresponding to (b), (f) blending noise corresponding to (c), (g) estimation error corresponding to (a), (h) estimation error corresponding to (b), and (i) estimation error corresponding to (c).

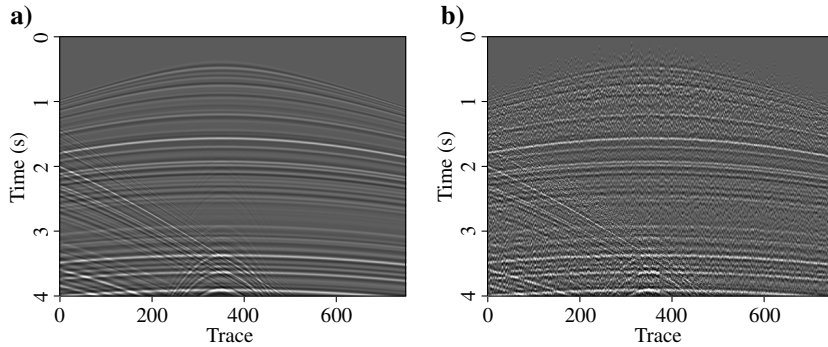


Figure 9. Numerically blended synthetic data (complex gather). (a) Unblended data and (b) blended data.

obtained an increase from 1.00 to 5.50 dB for the first source and from 0.83 to 5.50 dB for the second source. The error sections for this field data test are not given because unblended data for this test contain much random noise, which cannot be estimated. However, from the point of view of random noise attenuation, which is concerned with the signal content of the denoised section and the randomness of the noise section, the deblending result of the field data test is acceptable. In this case, the percentage we use for the seislet-domain thresholding is 18%.

The main computational cost of the proposed approach lays on the forward and inverse seislet

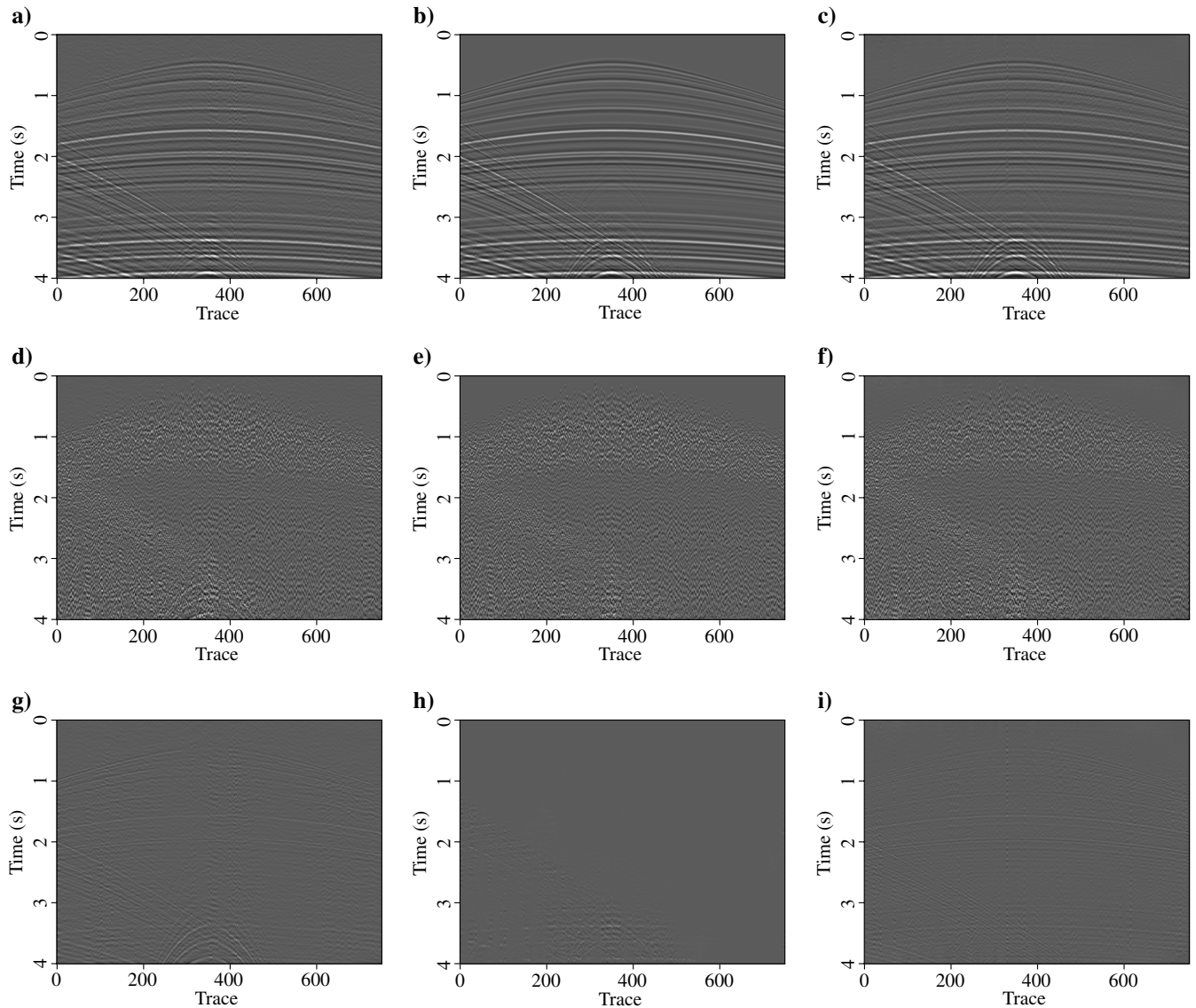


Figure 10. Deblending comparison for numerically blended synthetic data (complex gather). (a) Deblended result using $f\text{-}k$ domain thresholding, (b) deblended result using seislet-domain thresholding, (c) deblended result using $f\text{-}x$ predictive filtering, (d) blending noise corresponding to (a), (e) blending noise corresponding to (b), (f) blending noise corresponding to (c), (g) estimation error corresponding to (a), (h) estimation error corresponding to (b), and (i) estimation error corresponding to (c).

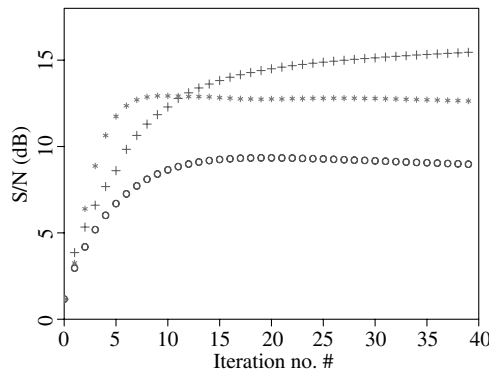


Figure 11. Diagrams of S/N for synthetic example (complex gather). The + line corresponds to seislet-domain thresholding, o line corresponds to $f\text{-}k$ domain thresholding, and the * line corresponds to $f\text{-}x$ predictive filtering.

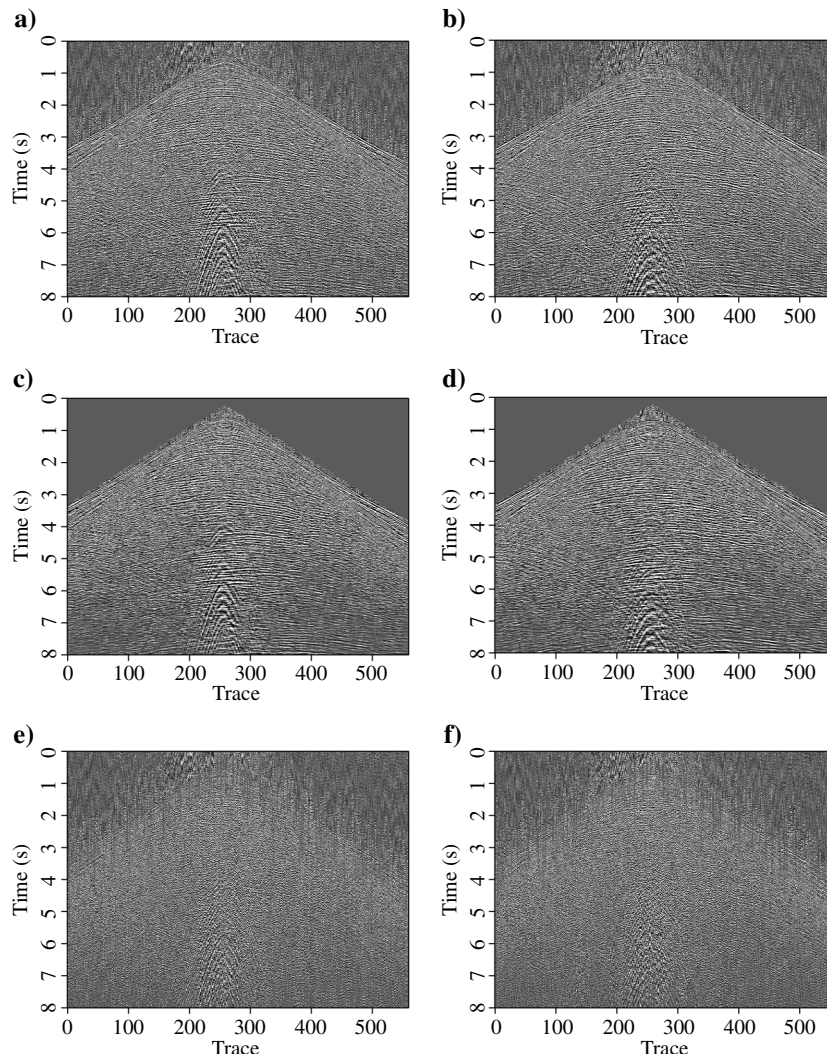


Figure 12. Deblending comparison for the real data. (a) Blended source 1, (b) blended source 2, (c) deblended source 1, (d) deblended source 2, (e) blending noise for source 1, and (f) blending noise for source 2.

transforms. As analyzed by Fomel and Liu (2010), the seislet transform has linear $O(N)$ cost. It can be more expensive than fast Fourier transform and digital wavelet transform, but is still comfortably efficient in practice. Considering that for the 2D seislet transform, the main cost may not be in the transform itself but in the iterative estimation of the slope fields, we update slope estimation every several iterations (e.g., every five iterations in this field data example) to reduce the computational cost.

CONCLUSIONS

We have proposed a novel iterative framework that offers a flexible way to control deblending using sparsity or coherency constraints. When the seismic data are relatively clean and do not contain much coherent noise, $f\text{-}k$ domain sparsity-promoting operator or $f\text{-}x$ predictive filtering might be adequate to handle the blending noise. However, when the blended data become more complicated, a more robust sparsity or coherency-promoting tool should be used. The seislet transform has an inherent ability to compress coherent seismic data because it is generated based on predictability between neighboring traces using the local slope information. As long as we can get an acceptable slope estimation, the seislet-transformed data appear sparse. Our experiments indicate that it is possible to get accurate results within a small number of iterations when an appropriate shaping operator is taken.

ACKNOWLEDGMENTS

We thank FairfieldNodal for providing the field data used in this study. We thank A. Klokov, K. Schleicher, P. Karimi, A. Mahdad, J. Paffenholz, D. Hays, P. Docherty, and L.-W. Mo for helpful discussions. We also thank S. Kaplan, C. Li, J. Cheng, J. Shragge, E. Slob, and one anonymous reviewer for their constructive suggestions, which helped to improve this paper.

APPENDIX A

REVIEW OF SEISLET TRANSFORM

Fomel (2006) and Fomel and Liu (2010) propose a digital wavelet like transform, which is defined with the help of the wavelet-lifting scheme (Sweldens, 1995) combined with local PWD. The wavelet lifting uses predictability of even traces from odd traces of 2D seismic data and finds a difference \mathbf{r} between them, which can be expressed as

$$\mathbf{r} = \mathbf{o} - \mathbf{P}[\mathbf{e}], \quad (\text{A-1})$$

where \mathbf{P} is the prediction operator. A coarse approximation \mathbf{c} of the data can be achieved by updating the even component:

$$\mathbf{c} = \mathbf{e} + \mathbf{U}[\mathbf{r}], \quad (\text{A-2})$$

where \mathbf{U} is the updating operator.

The digital wavelet transform can be inverted by reversing the lifting-scheme operations as follows:

$$\mathbf{e} = \mathbf{c} - \mathbf{U}[\mathbf{r}] \quad (\text{A-3})$$

and

$$\mathbf{o} = \mathbf{r} + \mathbf{P}[\mathbf{e}]. \quad (\text{A-4})$$

The forward transform starts with the finest scale (the original sampling) and goes to the coarsest scale. The inverse transform starts with the coarsest scale and goes back to the finest scale. At the start of forward transform, \mathbf{e} and \mathbf{o} corresponds to the even and odd traces of the data domain. At the start of the inverse transform, \mathbf{c} and \mathbf{r} will have just one trace of the coarsest scale of the seislet domain.

The above prediction and update operators can be defined, e.g., as follows:

$$\mathbf{P}[\mathbf{e}]_k = \frac{\mathbf{P}_k^{(+)}[\mathbf{e}_{k-1}] + \mathbf{P}_k^{(-)}[\mathbf{e}_k]}{2} \quad (\text{A-5})$$

and

$$\mathbf{U}[\mathbf{r}]_k = \frac{\mathbf{P}_k^{(+)}[\mathbf{r}_{k-1}] + \mathbf{P}_k^{(-)}[\mathbf{r}_k]}{4}, \quad (\text{A-6})$$

where $\mathbf{P}_k^{(+)}$ and $\mathbf{P}_k^{(-)}$ are operators that predict a trace from its left and right neighbors, correspondingly, by shifting seismic events according to their local slopes. This scheme is analogous to Cohen-Daubechies-Feauveau biorthogonal wavelets (Cohen et al., 1992). The predictions need to operate at different scales, which means different separation distances between traces. Taken through different scales, equations A-1–A-6 provide a simple definition for the 2D seislet transform. More accurate versions are based on other schemes for the digital wavelet transform (Liu et al., 2009a).

REFERENCES

- Abma, R. L., T. Manning, M. Tanis, J. Yu, and M. Foster, 2010, High quality separation of simultaneous sources by sparse inversion: 72nd Annual International Conference and Exhibition, EAGE, Extended Abstracts, B003.
- Abma, R., Q. Zhang, A. Arogunmati, and G. Beaudoin, 2012, An overview of BP's marine independent simultaneous source field trials: 82nd Annual International Meeting, SEG, Expanded Abstracts, doi: [10.1190/segam2012-1404.1](https://doi.org/10.1190/segam2012-1404.1).
- Beasley, C. J., B. Dragoset, and A. Salama, 2012, A 3D simultaneous source field test processed using alternating projections: A new active separation method: Geophysical Prospecting, **60**, 591–601, doi: [10.1111/j.1365-2478.2011.01038.x](https://doi.org/10.1111/j.1365-2478.2011.01038.x).
- Berkhout, A. J., 2008, Changing the mindset in seismic data acquisition: The Leading Edge, **27**, 924–938, doi: [10.1190/1.2954035](https://doi.org/10.1190/1.2954035).
- Berkhout, A. J., D. J. Verschuur, and G. Blacquiere, 2012, Illumination properties and imaging promises of blended, multiple-scattering seismic data: A tutorial: Geophysical Prospecting, **60**, 713–732, doi: [10.1111/j.1365-2478.2012.01081.x](https://doi.org/10.1111/j.1365-2478.2012.01081.x).
- Canales, L., 1984, Random noise reduction: 54th Annual International Meeting, SEG, Expanded Abstracts, 525–527.
- Candes, E. J., and Y. Plan, 2011, A probabilistic and RIPless theory of compressed sensing: IEEE Transactions on Information Theory, **57**, 7235–7254, doi: [10.1109/TIT.2011.2161794](https://doi.org/10.1109/TIT.2011.2161794).
- Chen, Y., and J. Ma, 2014, Random noise attenuation by f - x empirical mode decomposition predictive filtering: Geophysics, **79**, no. 3, V81–V91, doi: [10.1190/geo2013-0080.1](https://doi.org/10.1190/geo2013-0080.1).
- Choi, Y., and T. Alkhalifah, 2012, Application of multi-source waveform inversion to marine streamer data using the global correlation norm: Geophysical Prospecting, **60**, 748–758, doi: [10.1111/j.1365-2478.2012.01079.x](https://doi.org/10.1111/j.1365-2478.2012.01079.x).
- Cohen, A., I. Daubechies, and J. C. Feauveau, 1992, Biorthogonal bases of compactly supported wavelets: Communications on Pure and Applied Mathematics, **45**, 485–560, doi: [10.1002/cpa.3160450502](https://doi.org/10.1002/cpa.3160450502).
- Daubechies, I., M. Defrise, and C. D. Mol, 2004, An iterative thresholding algorithm for linear inverse problems with a sparsity constraint: Communications on Pure and Applied Mathematics, **57**, 1413–1457, doi: [10.1002/cpa.20042](https://doi.org/10.1002/cpa.20042).
- Daubechies, I., M. Fornasier, and I. Loris, 2008, Accelerated projected gradient method for linear inverse problems with sparsity constraints: Journal of Fourier Analysis and Applications, **14**, 764–792, doi: [10.1007/s00041-008-9039-8](https://doi.org/10.1007/s00041-008-9039-8).
- Donoho, D. L., 1995, De-noising by soft-thresholding: IEEE Transactions on Information Theory, **41**, 613–627, doi: [10.1109/18.382009](https://doi.org/10.1109/18.382009).
- Donoho, D. L., and I. M. Johnstone, 1994, Ideal spatial adaptation by wavelet shrinkage: Biometrika, **81**, 425–455, doi: [10.1093/biomet/81.3.425](https://doi.org/10.1093/biomet/81.3.425).
- Doulgeris, P., K. Bube, G. Hampson, and G. Blacquiere, 2012, Convergence analysis of a coherency-constrained inversion for the separation of blended data: Geophysical Prospecting, **60**, 769–781, doi: [10.1111/j.1365-2478.2012.01088.x](https://doi.org/10.1111/j.1365-2478.2012.01088.x).
- Fomel, S., 2002, Application of plane-wave destruction filters: Geophysics, **67**, 1946–1960, doi: [10.1190/1.1527095](https://doi.org/10.1190/1.1527095).
- Fomel, S., 2006, Towards the seislet transform: 76th Annual International Meeting, SEG, Expanded Abstracts, 2847–2850.
- Fomel, S., 2007, Shaping regularization in geophysical-estimation problems: Geophysics, **72**, no. 2, R29–R36, doi: [10.1190/1.2433716](https://doi.org/10.1190/1.2433716).
- Fomel, S., 2008, Nonlinear shaping regularization in geophysical inverse problems: 78th Annual International Meeting, SEG, Expanded Abstracts, 2046–2051.
- Fomel, S., and Y. Liu, 2010, Seislet transform and seislet frame: Geophysics, **75**, no. 3, V25–V38, doi: [10.1190/1.3380591](https://doi.org/10.1190/1.3380591).
- Galbraith, M., and Z. Yao, 2012, FX plus deconvolution for seismic data noise reduction: 82nd Annual International Meeting, SEG, Expanded Abstracts, doi: [10.1190/segam2012-1421.1](https://doi.org/10.1190/segam2012-1421.1).
- Gao, J., X. Chen, G. Liu, and J. Ma, 2010, Irregular seismic data reconstruction based on exponential threshold model of POCS method: Applied Geophysics, **7**, 229–238, doi: [10.1007/s11770-010-0246-5](https://doi.org/10.1007/s11770-010-0246-5).
- Guitton, A., and E. Diaz, 2012, Attenuating crosstalk noise with simultaneous source full waveform inversion: Geophysical Prospecting, **60**, 759–768, doi: [10.1111/j.1365-2478.2011.01023.x](https://doi.org/10.1111/j.1365-2478.2011.01023.x).
- Hampson, G., J. Stefani, and F. Herkenhoff, 2008, Acquisition using simultaneous sources: The Leading Edge, **27**, 918–923, doi: [10.1190/1.2954034](https://doi.org/10.1190/1.2954034).
- Hennfent, G., and F. Herrmann, 2006, Seismic denoising with nonuniformly sampled curvelets: Computing in Science & Engineering, **8**, 16–25.
- Huo, S., Y. Luo, and P. G. Kelamis, 2012, Simultaneous sources separation via multidirectional vector-median filtering: Geophysics, **77**, no. 4, V123–V131, doi: [10.1190/geo2011-0254.1](https://doi.org/10.1190/geo2011-0254.1).
- Liu, Y., 2013, Noise reduction by vector median filtering: Geophysics, **78**, no. 3, V79–V87, doi: [10.1190/geo2012-0232.1](https://doi.org/10.1190/geo2012-0232.1).
- Liu, Y., and S. Fomel, 2012, Seismic data analysis using local time-frequency decomposition: Geophysical Prospecting, **60**, 1–17, doi: [10.1111/j.1365-2478.2011.00957.x](https://doi.org/10.1111/j.1365-2478.2011.00957.x).
- Liu, Y., S. Fomel, C. Liu, D. Wang, G. Liu, and X. Feng, 2009a, High-order seislet transform and its application of random noise attenuation: Chinese Journal of Geophysics, **52**, 2142–2151.
- Liu, Y., C. Liu, and D. Wang, 2009b, A 1D time-varying median filter for seismic random, spike-like noise elimination: Geophysics, **74**, no. 1, V17–V24, doi: [10.1190/1.3043446](https://doi.org/10.1190/1.3043446).
- Mahdad, A., 2012, Deblending of seismic data: Ph.D. thesis, TU Delft.
- Mahdad, A., P. Doulgeris, and G. Blacquiere, 2011, Separation of blended data by iterative estimation and subtraction of blending interference noise: Geophysics, **76**, no. 3, Q9–Q17, doi: [10.1190/1.3556597](https://doi.org/10.1190/1.3556597).
- Mahdad, A., P. Doulgeris, and G. Blacquiere, 2012, Iterative method for the separation of blended seismic data: Discussion on the algorithmic aspects: Geophysical Prospecting, **60**, 782–801, doi: [10.1111/j.1365-2478.2012.01084.x](https://doi.org/10.1111/j.1365-2478.2012.01084.x).
- Mallat, S. G., 2009, A wavelet tour of signal processing: The sparse way: Academic Press.
- Mitchell, S., C. Ray, E. Marc, D. Hays, and K. Craft, 2010, FairfieldNodal's excellent nodal adventure: 80th Annual International Meeting, SEG, Expanded Abstracts, 3740–3745.
- Moore, I., B. Dragoset, T. Ommundsen, D. Wilson, C. Ward, and D. Eke, 2008, Simultaneous source separation using dithered sources: 78th Annual International Meeting, SEG, Expanded Abstracts, 2806–2809.
- Naghizadeh, M., and M. D. Sacchi, 2010, Beyond alias hierarchical scale curvelet interpolation of regularly and irregularly sampled seismic data: Geophysics, **75**, no. 6, WB189–WB202, doi: [10.1190/1.3509468](https://doi.org/10.1190/1.3509468).

- Plessix, R.-E., G. Baeten, J. W. de Maag, F. ten Kroode, and Z. Ruijie, 2012, Full waveform inversion and distance separated simultaneous sweeping: A study with a land seismic data set: *Geophysical Prospecting*, **60**, 733–747, doi: [10.1111/j.1365-2478.2011.01036.x](https://doi.org/10.1111/j.1365-2478.2011.01036.x).
- Sacchi, M. D., and H. Kuehl, 2000, FX arma filters: 70th Annual International Meeting, SEG, Expanded Abstracts, 2092–2095.
- Sweldens, W., 1995, Lifting scheme: A new philosophy in biorthogonal wavelet constructions: Wavelet applications in signal and image processing III: Proceedings of SPIE, **2569**, 68–79, doi: [10.1117/12.217619](https://doi.org/10.1117/12.217619).
- Van Borselen, R., R. Baardman, T. Martin, B. Goswami, and E. Fromyr, 2012, An inversion approach to separating sources in marine simultaneous shooting acquisition-application to a Gulf of Mexico data set: *Geophysical Prospecting*, **60**, 640–647, doi: [10.1111/j.1365-2478.2012.01076.x](https://doi.org/10.1111/j.1365-2478.2012.01076.x).
- Wang, D., C. Liu, Y. Liu, and G. Liu, 2008, Application of wavelet transform based on lifting scheme and percentiles soft-threshold to elimination of seismic random noise: (in Chinese) *Progress in Geophysics*, **23**, 1124–1130.
- Wapenaar, K., J. van der Neut, and J. Thorbecke, 2012, Deblending by direct inversion: *Geophysics*, **77**, no. 3, A9–A12, doi: [10.1190/geo2011-0497.1](https://doi.org/10.1190/geo2011-0497.1).
- Xue, Z., Y. Chen, S. Fomel, and J. Sun, 2014, Imaging incomplete data and simultaneous-source data using least-squares reverse-time migration with shaping regularization: 84th Annual International Meeting, SEG, Expanded Abstracts.
- Yang, P., J. Gao, and W. Chen, 2012, Improved POCS interpolation using a percentage thresholding strategy and excessively zero-padded FFT: 82nd Annual International Meeting, SEG, Expanded Abstracts, 1–6.
- Yang, P., J. Gao, and W. Chen, 2013, On analysis-based two-step interpolation methods for randomly sampled seismic data: *Computers & Geosciences*, **51**, 449–461, doi: [10.1016/j.cageo.2012.07.023](https://doi.org/10.1016/j.cageo.2012.07.023).